## Highlights

- Energy-efficient PEO layers are explored using electrolyte design and preanodizing
- The anodic film and the nature of the electrolyte influence the consumed energy
- The earlier establishment of soft sparking is strongly influenced by the anodic film
- Preanodized PEO in silicate-polyphosphate electrolyte enables 66% of energy savings
- The corrosion response is not affected significantly by the pre-anodizing and/or the type of electrolyte

# Effects of pre-anodizing and phosphates on energy consumption and corrosion performance of PEO coatings on AA6082

M. Mohedano[1]*, B. Mingo[2], H. Mora-Sánchez[1], E. Matykina[1], R. Arrabal[1]

1 Departamento de Ingeniería Química y de Materiales, Facultad de Ciencias Químicas, Universidad Complutense, 28040, Madrid, Spain

2 Department of Materials, The University of Manchester, Oxford Road, M13 9PL, Manchester, UK

*Corresponding author. E-mail: mmohedan@ucm.es

## Abstract

A significant reduction in the energy consumption of Plasma Electrolytic Oxidation (PEO) coatings on AA6082 alloy was obtained using strategies based on electrolyte selection and a precursor anodic film. PEO coatings were developed on AA6082 in silicate-based electrolytes with different phosphate species without and with a precursor oxide layer. The electrical response and, therefore, the specific energy consumption depended on the phosphate species and most notably on the applied pretreatment. The best result was obtained after anodic pretreatment and PEO in silicate-polyphosphate electrolyte with a reduction up to ~66% in comparison with the most conventional treatment (direct PEO in orthophosphate electrolyte). The corrosion response is not affected significantly by the pre-anodizing treatment either for short or prolonged immersion times revealing that coatings synthesised under high-energy efficient conditions have comparable corrosion performance under aggressive corrosive environments compared to conventional PEO processes.

**Keywords:** Aluminium alloys; Plasma Electrolytic Oxidation; Anodizing; Phosphate Electrolyte; Energy Consumption; Corrosion;

## 1. Introduction

Plasma Electrolytic Oxidation (PEO) technique produces ceramic-like coatings with improved corrosion and wear resistance on a wide range of Al alloys by using environmentally friendly dilute electrolytes [1]. Nowadays, the major obstacle for wider application of PEO technology is its high cost, which is associated with the high energy consumption –current densities and voltages are typically of the order of 20 A/dm$^2$ and 400 V (rms)–, and low coating efficiency (~25% [2, 3]). The loss of the PEO process efficiency is mainly related to: *(i)* the dielectric breakdown of the film, promoting electronic conductivity and reactions that generate oxygen and *(ii)* an excessive oxygen evolution during discharges ascribed to non-Faradic processes, which involve formation and following oxidation of $H_2O_2$ in the ionized gas [2-4].

Recent strategies for energy savings include [4-7] *(i)* electrical parameters optimization (*e.g.* high frequency bipolar signals), *(ii)* cell geometry design (*e.g.* 25% energy savings can be achieved by reducing the anode-to-cathode distance), and *(iii)* conventional anodizing pretreatment, which leads to a faster establishment of "soft sparking" under AC conditions, increasing the coating growth rate [8,9]. In particular, promising results to overcome the cost limitations of the PEO technique were obtained in the case of voltage-controlled PEO coatings on pre-anodized aluminum alloys with reductions in energy savings up to ~50% compared to conventional treatments [10,11]. However, the studies are quite recent and there is a need to investigate other aspects like the effect of the electrolyte in the promotion of the “soft sparking”. In fact, to the best of the authors´ knowledge, there is no data available regarding the effect of type of phosphate on the specific energy consumption of PEO coatings and neither the combination of strategies based on electrolyte selection and preanodizing has been previously attempted.

The present work combines in a systematic way two strategies in order to reduce the specific energy consumption of PEO coatings on Al. These strategies are electrolyte selection and use of a precursor anodic film formed in sulphuric acid. The results bring important insights into the selection of silicate-phosphates electrolytes with possibilities of knowledge transfer to other PEO treated alloys (Mg and Ti) for a wide range of applications (*i.e.* from thermomechanical to bioengineering).

## 2. Material and methods

### 2.1. Material

Rectangular specimens (40 mm × 20 mm × 1.5 mm) of Aluminum wrought alloy AA6082-T6 (wt.%: 0.015 Zn, 0.62 Mn, 0.86 Si, 0.022 Cu, 0.25 Fe, 0.84 Mg, bal. Al) were etched in 20% NaOH (30 s) and desmutted in concentrated $HNO_3$ (30 s), rinsed in deionised water and dried in warm air.

### 2.2. Surface treatment based on anodizing techniques

A working area of ~ 3 $cm^2$ was defined by application of Lacquer 45 resin (MacDermid plc).

The 20 µm-thick anodic precursor film was formed in sulphuric acid (24.5 wt.%) during 800 s at 50 $mA/cm^2$ and ~20ºC.

PEO coatings (without and with porous precursor film) were obtained in three electrolytes containing 10.5 g/L $Na_2O(SiO_2)_x{\cdot}xH_2O$ (≥27% $SiO_2$, $\rho$=1.39 g/L) and 2.8 g/L KOH. Additions of 5 g/L of different phosphate species: orthophosphate (O) $Na_3PO_4 \cdot 12H_2O$, pyrophosphate (PR) $Na_4P_2O_7$, or polyphosphate (PL) $Na_6P_6O_{18}$ were made as required. PEO treatment was carried out using an EAC-S2000 power supply

(ET Systems electronic) with a 490V/-110V square waveform at 50 Hz , 50 Hz, 50% duty cycle and a current density limit, $j_{rms}$, of 500 mA/cm$^2$. The coatings were developed in a 2 L double-walled glass cell (cooled water was pumped in order to maintain the electrolyte temperature close to 20 °C). As the counter-electrode a sheet of type 316 stainless steel (7.5 × 15 cm) was used. The process was terminated 600 s after the current drop to obtain similar coating thicknesses.

### 2.3. Surface characterization

Cross-sectional morphologies were examined after standard metallographic preparation by scanning electron microscopy using a JEOL JSM-6400 instrument equipped with Oxford Link energy-dispersive X-ray (EDS) microanalysis hardware. Surface roughness was measured over a distance of 4 mm in five different locations using a Surtronic 25 tester (Taylor Hobson Precision) and TalyProfile software applying a Gaussian filter of 2.5 mm. The thickness of the coatings was measured with an eddy current metre Isoscope FMP10 (Fischer) equipped with FTA3.3H probe. The presented values are the average of 10 measurements taken at arbitrary locations.

### 2.4. Specific Energy consumption

The specific energy consumption was calculated by integration of the voltage-time and current-time transients acquired by the power supply (SM 400AR-8 Systems electronic, 2-channel Tektronix TDS 2012B oscilloscope at 100 MHz sampling rate) during the treatment and according to Equation 1. The total energy ($E_{TOTAL}$) is the energy consumed during the PEO process ($E_{PEO}$) and the anodizing process, where applicable ($E_{ANOD}$ is ~2.3 kW h m$^{-2}$). With the obtained results, the specific energy consumption in

$kW \cdot h \cdot m^{-2} \cdot \mu m^{-1}$ was obtained dividing $E_{TOTAL}$ by the final coating thickness. Results were calculated as an average of three specimens.

$$E_{TOTAL} = \int_{to}^{t} [V\ i]\ \left[\frac{W\ s}{m^2}\right] dt \quad (1)$$

Where $V$ is instantaneous voltage, $i$ is instantaneous current density, $t_0$ is the starting point of the experiment, $t$ is the end time of the experiment.

### 2.5. Corrosion performance

EIS measurements were conducted up to 14 d of immersion in naturally aerated 3.5 wt.% NaCl aqueous solution at (22 ± 0.5) °C using a Gill AC computer-controlled potentiostat. All potentials were measured with respect to Ag/AgCl reference electrode with 1 $cm^2$ of specimen exposed area and a graphite counter–electrode. A sinusoidal 10 mV amplitude perturbation in the frequency range of 30 kHz–0.01 Hz was applied in duplicated specimens to ensure repeatability.

## 3. Results and discussion

### 3.1. Electrical response and efficiency

Details of the voltage evolution during the development of the precursor anodic coating and the cross-section of the obtained layer are shown in Figure 1.

The voltage-time transient reveals a sharp peak at the beginning up to ~25 V that rapidly decreases reaching ~19 V after 30 s. This is followed by a gradual increase with time, reaching the final value of ~24 V at 800 s (Fig. 1a).

The backscattered scanning electron micrographs of the cross-section reveal an oxide layer with an average thickness of (20 ± 0.5) μm with no noticeable irregularities. The presence of second phases at the substrate/oxide interface do not block the growth of the oxide film having no negative effect on the morphology of the anodic layer.

Rms current-time transients during different PEO treatments show an effect of both the type of electrolyte and the precursor anodic film on the earlier establishment of "soft sparking" regime (Fig. 2). All PEO coatings reveal a current drop, which is a common feature under voltage-controlled mode associated with an increase of the coating impedance and therefore the higher resistance of the oxide material to mass transfer. Treatments were stopped 600 s after a drop in the current signal was observed which corresponded to the establishment of "soft sparking" over the entire specimen surface (600 s was an arbitrary selected time that ensured homogeneous coating thickness).

For direct PEO (Fig. 2 a), polyphosphate electrolyte shifts the current drop to shorter times (~1970 s) compared with pyrophosphate (~2340 s) and orthophosphate (~2600 s). The same trend was observed for coatings with precursor anodic layer: ~460 s (PL), ~980 s (PR) and ~1080 s (O), respectively (Fig. 2 b).

It is important to notice that up-to-date the relationship between PEO processing parameters and microdischarge properties remains somehow unclear and most studies only addressed the influence of the electrical aspects (voltage, current, pulse form, frequency and duty cycle) on the microdischarge regime and coating growth rate [12-14]. Results found in the present work provide new evidence on the latter point revealing a relation between the composition of the electrolyte and microdischarges characteristics affecting the establishment of "soft sparking". Differences may be attributed to a combination of different factors such as conductivity ($Na_3PO_4 \cdot 12H_2O$: 9.34 μS/cm, $Na_4P_2O_7$: 12.56 μS/cm and $Na_6P_6O_{18}$ 12.76 μS/cm), structure and bonding strength of phosphate species and the molar concentration of phosphorus element. In fact, findings addressed the increase of molar concentration of phosphorus element as the main factor contributing to an earlier establishment of soft sparking (orthophosphate: 0.013M, pyrophosphate: 0.037M and polyphosphate: 0.049 M). An increase of phosphorus concentration in the electrolyte and, subsequently, an increase of phosphorous content in the coating (P element EDS analysis of plan view in at.%: PEO-O: 0.34, PEO-PR: 0.48 and PEO-PL 0.75) may promote the earlier "soft sparking" establishment by affecting the physical properties of the coating such as ionic and thermal conductivity. Differences in discharge characteristics of PEO processes conducted in several phosphate-silicate mixture electrolytes were also observed by Y. Mori et al., and they were attributed to different reactivity of the substrate with ions of electrolyte such as $PO_4^{3-}$ and $SiO_3^{2-}$ [15]

Unfortunately, up to date the knowledge about thermo-physical properties of PEO coatings and their relation with microstructure or processing conditions remain very limited. It was disclosed by Curran and Clyne [16] that thermal conductivity of PEO coated aluminum is relatively low compared to single crystal $Al_2O_3$ which was

attributed to the presence of a significant proportion of amorphous phase in the coating. In the present work and according to Matykina et al. [17] the incorporation of P into the PEO coatings promotes formation of amorphous phase and therefore a decrease in the thermal conductivity of the material can be expected which, in turn, may facilitate the overheating of the ionized gas and bring on the earlier contraction of the positive column of the plasma [8,18]. It is worthy to note that results found in the present work incentivize further investigations to determine the influence of amorphous phases on the thermo-physical properties of PEO coatings.

It has recently been demonstrated by Nominé et al. that surface charge of the coating material, which is dependent on the isoelectric point of the oxide (IEP) and the pH of the electrolyte (i.e., the species present in the electrolyte) affects the type of the microdischarges, promoting anodic or cathodic ones, when the pH of the electrolyte is, respectively, greater or lower than the IEP [19]. Specific adsorption of phosphate ions further assists the build-up of the excessive charge (by increasing the difference between the IEP of $Al_2O_3$ and the electrolyte pH) that leads to breakdown of the ceramic oxide and gas. A combination of these factors is probably taking place leading to earlier onset of "soft sparking". The longer the material is subjected to "soft sparking", the greater is the overall coating growth rate (Table 1).

Regardless of the electrolyte employed for the coatings formation, the presence of a precursor anodic film decreases significantly the time for establishment of uniform “soft sparking” by 2-4 times when compared with direct PEO (Fig. 2 b) which is in concordance with previous studies reporting that the transition to “soft sparking” occurs once a sufficient thickness of the coating has been achieved [8].

Relevant parameters of the studied PEO coatings without and with precursor film are gathered in Table 1. In terms of electric energy consumption, the total energy applied

($E_{TOTAL}$) is calculated as the sum of the energy spent during PEO process ($E_{PEO}$) and the energy consumed during preanodizing ($E_{ANOD}$) which is ~2.3 kW h $m^{-2}$.

In case of direct PEO treatments, a reduction of the consumed energy (kW h $m^{-2}$ $\mu m^{-1}$) by ~10% and ~18% is obtained for pyrophosphate and polyphosphate containing electrolytes, respectively, in comparison with the orthophosphate species and it is associated with the early establishment of the "soft sparking" regime.

Using the precursor anodic film a significant reduction in the consumed energy is achieved in comparison with direct PEO developed in the same electrolyte (~57% for A+PEO-O, ~57 % for A+PEO-PR and ~58% A+PEO-PL). Notably, not only the anodic film but also the nature of the electrolyte influences the total consumed energy following the same trend as in the case of direct PEO (PEO-O>PEO-PR >PEO-PL). A reduction of the energy consumed by ~12% and ~20% were obtained for PEO coatings with anodic precursor film conducted in pyrophosphate and polyphosphate electrolytes in comparison with the orthophosphate based electrolyte. These values are similar to the ones obtained in the case of direct PEO and point out the influence of phosphate species in the electrolyte on the energy consumption regardless of the precursor anodic film pre-treatment.

In general, findings reveal a remarkable improvement compared with the data available for different modes of PEO process of commercial aluminum alloys [20] (e.g. the specific energy consumption silicate–phosphate electrolytes may be as high as 26.7 kW h $m^{-2}$ $\mu m^{-1}$). The most promising results are found for PEO coating with anodic precursor film developed in polyphosphate electrolyte with an energy savings up to ~ 66% compared to conventional direct PEO treatment formed in orthophosphate electrolyte.

### 3.2. Morphology and composition

SEM surface views of all coated specimens are shown in Figure 3 along with the surface area analysis (Table 2).

All the coatings reveal the typical surface morphology of plasma electrolytic oxidation layers with some micro-cracks and pores at the sites of the discharge channels associated with thermal stresses and gas evolution through the molten oxide material during the PEO treatment [1]. The precursor anodic film does not influence significantly the final surface morphology of the coatings. It is worth noting that the surface roughness of the coatings (Table 2) and the number of transversal cracks (Fig. 5) slightly decrease when increasing the concentration of phosphorous in the electrolyte. The semi-quantitative analyses of the elemental composition of the coatings performed by EDS (Table 2) disclose that the oxide layers incorporated elements from the substrate (Mn) and from the electrolyte (Si, P, Na, K). The slightly increase of phosphorous content in the coating might be related with the increase of phosphorus concentration in the electrolyte. A very low residual amount of S is observed for the oxide layers formed with an anodic (sulfur based) precursor film.

X-ray diffraction analysis (Fig. 4) reveal that all the coatings are mainly formed by α-$Al_2O_3$, γ-$Al_2O_3$ and $3Al_2O_3 \cdot 2SiO_2$ (mullite), with minor amounts of $AlPO_4$. The preanodized coatings contain a slightly higher proportion of $AlPO_4$, as deduced from the higher intensity of the diffraction peaks. This is consistent with the EDS analysis where slightly higher values of P were also identified (Table 2). It is worth noting that A+PEO-O is the one that presents the lower amount of P out of the three of them. The formation of compounds derived from species present in the electrolyte, such as

phosphates, is associated with microdischarges that take place near the coating surface that promote their incorporation [4].

The cross section of the studied coatings show a thickness in a range of 62-85 μm depending on the treatment and consist of a three-layered structure (highly-porous outer part, denser intermediate layer with smaller porosity and a sub-micron size barrier layer). The PEO coating growth rates on pre-anodized alloys were in general 1.7 times higher than on non-pre-anodized. The lowest values were obtained for treatments conducted in orthophosphate baths.

The partial transformation of the preformed anodic film during PEO process is disclosed in Figure 6 corresponding to different times of the process (from 60 s to 1000 s) of A+PEO-PL and A+PEO-O coatings. Up to 200 s of PEO treatment, similar features are observed for the plasma dielectric breakdown events of both coatings, characterized with a non-uniform transformation of the anodic layer into PEO morphology. For longer treatment times (300 s), the differences between the two electrolytes are more evident with an almost total transformation of the anodic film for the A+PEO-PL in comparison with the un-modified larger area of the anodic film for A+PEO-O. After 400 s, the coating developed into polyphosphate electrolyte reveals a homogeneous PEO layer, which is in concordance with the current drop observed at 460 s (Figure 2b). The total transformation of the anodic film into and homogeneous PEO coating is observed after 1000 s of treatment as it was expected from the current drop at ~1080 s (Figure 2b)

A more detailed study of the partial transformation of the preformed anodic film during PEO-O process is presented in Figure 7 with the corresponding X-ray elemental mapping (S, Si) and local EDS analysis for the higher magnification detail (Table 2).

The micrographs correspond to 400 s of PEO process, when the pre-formed anodic film was only partly converted into the PEO coating. EDS point analysis at location 1 corresponds to the remaining anodic film unaffected by microdischarges (Figure 7b, Table 3). The analysis shows elements characteristic of the anodic film developed in sulphuric acid (Al, O and S) and elements incorporated from the substrate (Mn). In the areas affected by the microdischarges, EDS analyses at locations 2 and 3, S content was reduced and the amount of Na, K, P and Si increased, which is in concordance with the typical composition of PEO coatings developed in mixed electrolytes [21]. Element distribution maps are consistent with the EDS analysis, showing S-rich regions in the remaining pre-formed anodic film and Si near the coating surface, confirming that during the PEO treatment the anodic precursor layer is transformed in composition, structure and morphology. It is worth mentioning that the continuous thin S-rich layer observed underneath the PEO coating reveals a very recessed interface indicating that the original anodic layer underwent a transformation during the growth of the PEO coating [22]. Although this S-rich film is not observed at later stages when "soft sparking" overtakes completely, its presence could be detrimental for corrosion properties. Therefore, the underlayer growth deserves further detailed studies. In addition, deeper investigations using this S-rich underlayer as a tracer could help to clarify the growth mechanisms of the PEO coatings. For instance, Monfort et al. [23] characterized for the first time a continuous thin amorphous alumina film in the interlayer substrate/coating next to the metal/coating interface and more recently Zhu et al. [24] proposed a mechanism for the growth of PEO coating involving the amorphous alumina layer next to the substrate and ionic migration processes. In this regard, the detailed transformation of the alumina precursor film during the PEO treatment could

be a useful tool in a future work for better understanding of the growth mechanism of this type of coatings.

### 3.3 Corrosion evaluation

The electrical response results showed that the appropriate selection of the electrolyte and pre-anodizing step leads to a considerable reduction in energy consumption. However, it is of paramount importance to ensure that the physical integrity of the coatings and therefore their performance is not affected by such reduction. Electrochemical Impedance Spectroscopy (EIS) was used to evaluate the corrosion resistance in naturally aerated NaCl 3.5 wt.% solution up to 14 days of immersion. Figure 8 shows the modulus of impedance at low frequencies which provides a good estimation of the overall corrosion performance of the material. The corrosion resistance of the coatings tends to decrease with time and the steepest drop occurs after 3 h-1 d. In case of PEO-PL and A+PEO-PL, a slight increase can be identified just before the drop after 1 d and 3h, respectively; this is probably associated with the aluminium passivation and/or precipitation of corrosion products at open microdefects at the substrate/coating interface that provide partial and temporary corrosion protection. It is evident from Figure 8 that the corrosion resistance of the coatings synthesized in PR and PL electrolytes present a higher corrosion resistance, especially at short immersion times (1 d). However, at prolonged times (14 d), the improvement of the corrosion resistance is not as significant and the $|Z|_{0.01Hz}$ values remain in the same order of magnitude for all the studied coatings.

Figure 9 shows the Bode plots after 14 days of immersion and compares the influence of the anodic precursor and the composition of the electrolyte used during the synthesis of the coatings. The corrosion resistance of the preanodized specmens is slightly higher

than that observed for direct PEO, although the improvement is not significant. However, it is evident from Figure 9a that the presence of the anodic precursor modifies the EIS response of the material. Direct PEO coatings show one time constant at low-intermediate frequencies (1-10 Hz) associated with the resistive-capacitive behaviour of the coating. On the contrary, the preanodized specimenes clearly show two time constants at intermediate ($10^2$ Hz) and low (10 Hz) frequencies. The one at higher frequencies is associated with the compact inner barrier layer and the one at lower frequencies is attributable to the capacitive behaviour of the double electric layer and to the charge transfer resistance at the substrate/oxide interface [25]. This could be related to the formation of a thicker inner barrier layer in the preanodized specimens associated to the earlier establishment of the soft sparking regime, which is in agreement with previous results obtained by the authors on a rheocast A356 aluminium alloy [11]. Figure 9b shows the influence of the electrolyte composition on the EIS response. For both,direct and preanodized PEO specimens the orthophosphate rich electrolyte (O) leads to the lowest $|Z|_{0.01Hz}$ response, while pyro (PR) and polyphosphate (PL) yield similar results. Such slight improvement can be related to the higher amount of phosphorous in the electrolytes, which reduces slightly the surface roughness and number of transversal cracks and voids of the coatings that could act as potential paths for electrolyte access.

The EIS study revealed that coatings synthesised under high-energy efficient conditions have comparable corrosion performance to that of conventional PEO processes. In fact, substantial improvements were achieved for specific combinations of pre-anodizing treatment and electrolyte (A+PEO-PL). This evidences that it is indeed possible to develop low energy consumption PEO coatings without affecting negatively their corrosion performance.

## 4. Conclusions

1. The establishment of "soft sparking" over the entire specimen surface is influenced by both the electrolyte and the precursor anodic film, the influence of the latter being significantly greater.
2. The best results in terms of energy savings were obtained for the preanodized specimen PEO-treated AA6082 alloy in the presence of polyphosphate (~3.2 kW h $m^{-2}$ $\mu m^{-1}$ and ~66% energy savings). The least efficient was ortophosphate (~9.3 kW h $m^{-2}$ $\mu m^{-1}$).
3. PEO coating growth rates were ~1.7 times higher on pre-anodized specimens compared to direct PEO. The lowest values were found for treatments conducted in the presence of orthophosphate.
4. The corrosion response is not affected significantly by the pre-anodizing treatment either for short or prolonged immersion times. However, the optimum selection of the electrolyte can indeed increase noticeably the overall corrosion response as observed for A+PEO-PL. This confirms that it is possible to develop low-energy consumption PEO coatings, while maintaining similar corrosion properties of conventional PEO coatings.

**Acknowledgements**

The authors gratefully acknowledge the support of the RTI2018-096391-B-C33 (MCIU/AEI/FEDER, UE) and ADITIMAT-CM (S2018/NMT-4411) projects. M. Mohedano and H. Mora-Sánchez are grateful for the support of RYC-2017 21843 and PEJD-2019-POST/IND-16119 respectively. The technical support from Ms. Y. Llamazares and the scientific discussion with Prof. A. Pardo are gratefully acknowledged.

## References


1. A.L. Yerokhin, X. Nie, A. Leyland, A. Matthews, Plasma electrolysis for surface engineering, Surf. Coat. Technol. 122 (1999) 73-93. https://doi.org/10.1016/S0257-8972(99)00441-7

2. L.O Snizhko, A. L Yerokhin, A. Pilkington, N.L Gurevina, D.O. Misnyankin, A. Leyland, A. Matthews, Anodic processes in plasma electrolytic oxidation of aluminium in alkaline solutions, Electrochim. Acta 49 (2004) 2085-2095. https://doi.org/10.1016/j.electacta.2003.11.027

3. L.O Snizhko, A.L Yerokhin, N.L Gurevina, V.A. Patalakha, A. Matthews, Excessive oxygen evolution during plasma electrolytic oxidation of aluminium, Thin Solid Films 516 (2007) 460-464. https://doi.org/10.1016/j.tsf.2007.06.158

4. E. Matykina, R. Arrabal, M. Mohedano, B. Mingo, J. Gonzalez, A. Pardo, M.C. Merino, Recent advances in energy efficient PEO processing of aluminium alloys, Trans. Nonferrous Met. Soc. China 27(2017) 1439-1454. https://doi.org/10.1016/S1003-6326(17)60166-3

5. T.W. Clyne, S.C. Troughton, A review of recent work on discharge characteristics during plasma electrolytic oxidation of various metals, Int. Mater. Rev. (2018). https://doi.org/10.1080/09506608.2018.1466492

6. X.M. Zhang, X.B. Tian, S.Q. Yang, C.Z. Gong, R.K. Fu, P.K. Chu, Low energy-consumption plasma electrolytic oxidation based on grid cathode. Rev. Sci. Instrum. 81 (2010) 103504. doi: 10.1063/1.3500319

7. V. Dehnavi, B.L. Luan, D.W. Shoesmith, X.Y. Liu, Effect of duty cycle and applied current frequency on plasma electrolytic oxidation (PEO) coating growth behavior, S. Rohani, Surf. Coat. Technol. 226 (2013) 100-107. https://doi.org/10.1016/j.surfcoat.2013.03.041

8. E. Matykina, R. Arrabal, P. Skeldon, G.E. Thompson, P. Belenguer, AC PEO of aluminium with porous alumina precursor films, Surf. Coat. Technol. 205 (2010) 1668-1678. https://doi.org/10.1016/j.surfcoat.2010.05.014

9. E. Matykina, R. Arrabal, A. Mohamed, P. Skeldon, G.E. Thompson, Plasma electrolytic oxidation of pre-anodized aluminium, Corr. Sci. 51 (2009) 2897-2905. https://doi.org/10.1016/j.corsci.2009.08.004

10. E. Matykina, R. Arrabal, A. Pardo, M. Mohedano, B. Mingo, I. Rodriguez, J. Gonzalez, Energy-efficient PEO process of aluminium alloys, Mater. Lett. (2014) 13-16. https://doi.org/10.1016/j.matlet.2014.04.077

11. M. Mohedano, E. Matykina, R. Arrabal, B. Mingo, M.L. Zheludkevich, PEO of rheocast A356 Al alloy: energy efficiency and corrosion properties, Surf. Interface Anal. 48 (2016) 953-959. https://doi.org/10.1002/sia.5815

12. F. Jaspard-Mécuson, T. Czerwiec, G. Henrion, T. Belmonte, L. Dujardin, A. Viola, J. Beauvir, Tailored aluminium oxide layers by bipolar current adjustment in the Plasma Electrolytic Oxidation (PEO) process, Surf. Coat. Technol. 201 (2007) 8677-8682. https://doi.org/10.1016/j.surfcoat.2006.09.005

13. J. Martin, A. Melhem, I. Shchedrina, T. Duchanoy, A. Nominé, G. Henrion, T. Czerwiec, T. Belmonte, Effects of electrical parameters on plasma electrolytic oxidation of aluminium, Surf. Coat. Technol. 221 (2013) 70-76. https://doi.org/10.1016/j.surfcoat.2013.01.029

14. J. Martin, A. Nominé, F. Brochard, J-L. Briançon, C. Noël, T. Belmonte, T. Czerwiec, G. Henrion, Delay in micro-discharges appearance during PEO of Al: Evidence of a mechanism of charge accumulation at the electrolyte/oxide interface, Appl. Surf. Sci. 410 (2017) 29-41. https://doi.org/10.1016/j.apsusc.2017.03.088

15. Y. Mori, A. Koshi, J. Liao, H. Asoh, S. Ono, Characteristics and corrosion resistance of plasma electrolytic oxidation coatings on AZ31B Mg alloy formed in phosphate – Silicate mixture electrolytes, Corr. Sci. 88 (2014) 254-262. https://doi.org/10.1016/j.corsci.2014.07.038

16. J.A. Curran, T.W. Clyne, The thermal conductivity of plasma electrolytic oxide coatings on aluminium and magnesium, Surf. Coat. Technol. 199 (2005) 177-183. https://doi.org/10.1016/j.surfcoat.2004.11.045

17. E. Matykina, F. Monfort, A. berkani, P. Skeldon, G.E. Thompson, J. Gough, Characterization of spark-anodized titanium for biomedical applications, J. Electrochem. Soc. 154 (2007) 279-285. DOI: 10.1149/1.2717383

18. V.V. Bakovets, O.V. Polyakov, I.P. Dolgovesova, Nauka, Novosibirsk, 1991 (In Russian)

19. A. Nomine, J. Martin, C. Noël, G. Henrion, T. Belmonte, I.V. Bardin, P. Lukes, Surface Charge at the Oxide/Electrolyte Interface: Toward Optimization of Electrolyte Composition for Treatment of Aluminum and Magnesium by Plasma Electrolytic Oxidation, Langmuir 32 (2016) 1405-1409. DOI**:** 10.1021/acs.langmuir.5b03873

20. L. Yerokhin, A. Shatrov, V. Samsonov, P. Shashkov, A.Pilkington, A. Leylan, A. Matthews, Oxide ceramic coatings on aluminium alloys produced by a pulsed bipolar plasma electrolytic oxidation process, Surf. Coat. Technol. 199 (2005) 150-157. https://doi.org/10.1016/j.surfcoat.2004.10.147

21. G. Lv, W. Gu, H. Chen, W. Feng, M. L. Khosa, L. Li, E. Niu, G. Zhang, S. Yang, Characteristic of ceramic coatings on aluminum by plasma electrolytic oxidation in silicate and phosphate electrolyte, Appl. Surf. Sci. 253 (2006) 2947-2952. https://doi.org/10.1016/j.apsusc.2006.06.036

22. E. Matykina, R. Arrabal, A. Mohamed, P. Skeldon, G.E. Thompson, Plasma electrolytic oxidation of pre-anodized aluminium, Corr. Sci. 51 (2009) 2897-2905. https://doi.org/10.1016/j.corsci.2009.08.004

23. F. Monfort, A. Berkani, E. Matykina, P. Skeldon, G.E. Thompson, H. Habazaki, K. Shimizu, Development of anodic coatings on aluminium under sparking conditions in silicate electrolyte, Corr. Sci. 49 (2007) 672-693. https://doi.org/10.1016/j.corsci.2006.05.046

24. L. Zhu, Z. Guo, Y. Zhang, Z. Li, M. Sui, A mechanism for the growth of a plasma electrolytic oxide coating on Al, Electrochim. Acta, 208 (2016) 296-303. https://doi.org/10.1016/j.electacta.2016.04.186

25. Z. Yang, X. Zhang, Y. Wu, G. Wu, D. Wang, X. Liu, H. Han, Y. Shen, The correlation between the Na2SiO3·9H2O concentrations and the characteristics of plasma electrolytic oxidation ceramic coatings, Ceramics International 45 (2019) 19388-19394. https://doi.org/10.1016/j.ceramint.2019.06.191

**Figures**

**Figure 1**. Figure 1. (a) voltage-time transient of anodizing in sulphuric acid (24.5 wt.%) at 50 mA/cm$^2$ and ~20ºC. Backscattered electron images of the anodic layer cross-sections (b) lower magnification (c) higher magnification.

**Figure 2**. Rms current-time transients of PEO in different electrolytes for (a) direct PEO (b) PEO with precursor anodic film. Voltage values are also included for the electrolytes containing orthophosphate.

**Figure 3**. PEO coating surface view without precursor (a–c), and with precursors (d–f). Electrolytes: (a,d): ortophosphate (b,e): pyrophosphate (c,f): polyphosphate.

**Figure 4**. X-ray diffraction patterns of (a) PEO-O, PEO-PR and PEO-PL and (b) preanodized A+PEO-O, A+PEO-PR and A+PEO-PL coatings.

**Figure 5**. Backscattered electron images of the PEO coating cross-sections without precursor (a–c), and with precursors (d–f). Electrolytes: (a,d): silicate-ortophosphate (b,e): pyrophosphate (c,f): polyphosphate.

**Figure 6**. Partial transformation at different times of the preformed anodic film during PEO-O and PEO-PL process.

**Figure 7.** Backscattered electron micrographs of the PEO coating formed in silicate-orthophosphate electrolyte (400 s) with pre-anodized layer: (a) lower magnification, (b) higher magnification with its respective X-ray elemental maps of S and Si.

**Figure 8.** Total impedance at 0.01 Hz of the studied coatings as a function of the immersion time in naturally aerated NaCl 3.5 wt.% solution.

**Figure 9.** Bode plot of the studied coatings after 14 d of immersion in naturally aerated NaCl 3.5 wt. % solution as a function of (a) the anodic precursor and (b) electrolyte.

**Tables**

**Table 1.** Parameters of the PEO coatings obtained in studied electrolytes with and without precursor film (490V/-110V, 50 Hz, 500 mA/cm$^2$ current density limit). The process was terminated 600 s after the current drop to obtain similar coating thicknesses.

**Table 2.** Local EDS semi-quantitative analysis of the surface of different PEO coatings.

**Table 3**. Local EDS semi-quantitative analysis of the PEO coating obtained in orthophosphate electrolyte with a precursor film.

Table

**Table 1.** Parameters of the PEO coatings obtained in studied electrolytes with and without precursor film (490V/-110V, 50 Hz, 500 mA/cm$^2$ current density limit). The process was terminated 600 s after the current drop to obtain similar coating thicknesses.

| Treatment | $E_{PEO}$ (kW h m$^{-2}$) | $E_{TOTAL}$ (kW h m$^{-2}$μm$^{-1}$) | Thickness (μm) | Growth rate (μm min$^{-1}$) | $R_a$ (μm) |
|---|---|---|---|---|---|
| PEO-O | 790 ± 20 | 9.3 ± 1.3 | 85 ± 10 | 1.6 ± 0.2 | 5.2 ± 0.4 |
| PEO-PR | 663 ± 19 | 8.4 ± 1.2 | 79 ± 9 | 1.6 ± 0.3 | 4.4 ± 0.4 |
| PEO-PL | 569 ± 17 | 7.5 ± 0.7 | 75 ± 4 | 2.0 ± 0.1 | 4.3 ± 0.4 |
| A+PEO-O | 311 ± 9 | 4.0 ± 0.8 | 78 ± 15 | 2.8 ± 0.5 | 5.1 ± 0.4 |
| A+PEO-PR | 268 ± 8 | 3.5 ± 0.3 | 76 ± 4 | 2.9 ± 0.2 | 4.1 ± 0.3 |
| A+PEO-PL | 199 ± 6 | 3.2 ± 0.3 | 62 ± 6 | 3.4 ± 0.2 | 3.9 ± 0.4 |

**Table 2.** Local EDS semi-quantitative analysis of the surface of different PEO coatings.

| | Elements at. % | | | | | | | |
|---|---|---|---|---|---|---|---|---|
| Coating | O | Na | Al | Si | P | K | Mn | S |
| PEO-O | 61.67 | 1.71 | 21.46 | 11.72 | 0.34 | 3.06 | 0.06 | - |
| PEO-PR | 60.38 | 2.27 | 22.22 | 11.78 | 0.48 | 2.74 | 0.15 | - |
| PEO-PL | 61.35 | 1.52 | 21.46 | 11.98 | 0.75 | 2.99 | - | - |
| A+PEO-O | 61.66 | 1.84 | 22.53 | 10.48 | 0.35 | 2.83 | 0.16 | 0.13 |
| A+PEO-PR | 61.69 | 2.11 | 21.17 | 11.71 | 0.52 | 2.63 | 0.09 | 0.08 |
| A+PEO-PL | 61.92 | 1.68 | 20.02 | 12.46 | 0.66 | 3.14 | 0.08 | 0.03 |

**Table 3.** Local EDS semi-quantitative analysis of the PEO coating obtained in orthophosphate electrolyte with a precursor film.

| | Elements (at. %) | | | | | | | |
|---|---|---|---|---|---|---|---|---|
| Point | O | Na | Al | Si | P | K | Mn | S |
| 1 | 62.80 | - | 34.00 | 0.24 | - | - | 0.07 | 2.89 |
| 2 | 61.51 | 0.28 | 35.73 | 1.55 | 0.42 | 0.39 | - | 0.12 |
| 3 | 61.75 | 0.81 | 31.23 | 4.01 | 0.46 | 1.70 | - | 0.03 |

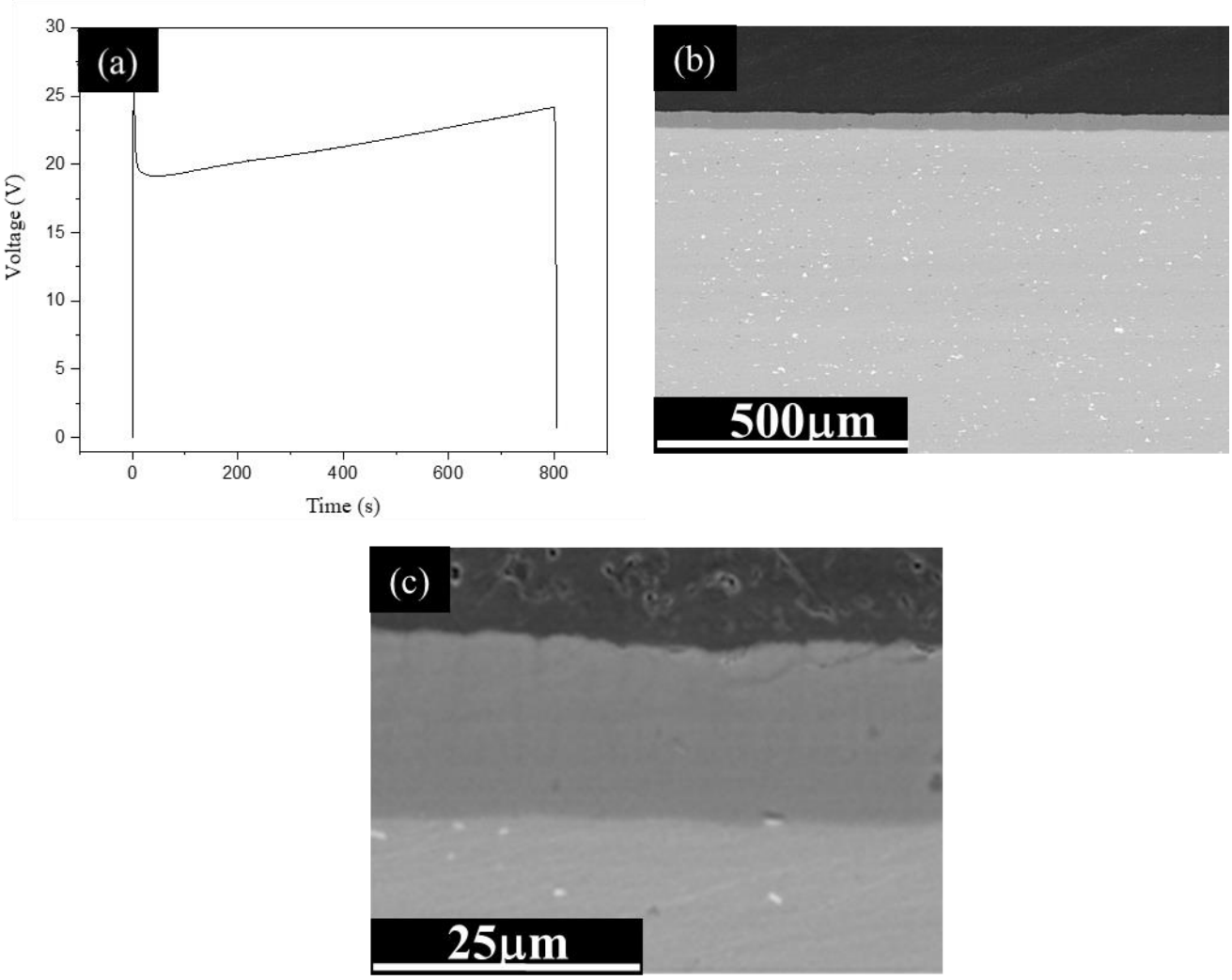


Figure 1. (a) voltage-time transient of anodizing in sulphuric acid (24.5 wt.%) at 50 mA/cm$^2$ and ~20ºC. Backscattered electron images of the anodic layer cross-sections (b) lower magnification (c) higher magnification.

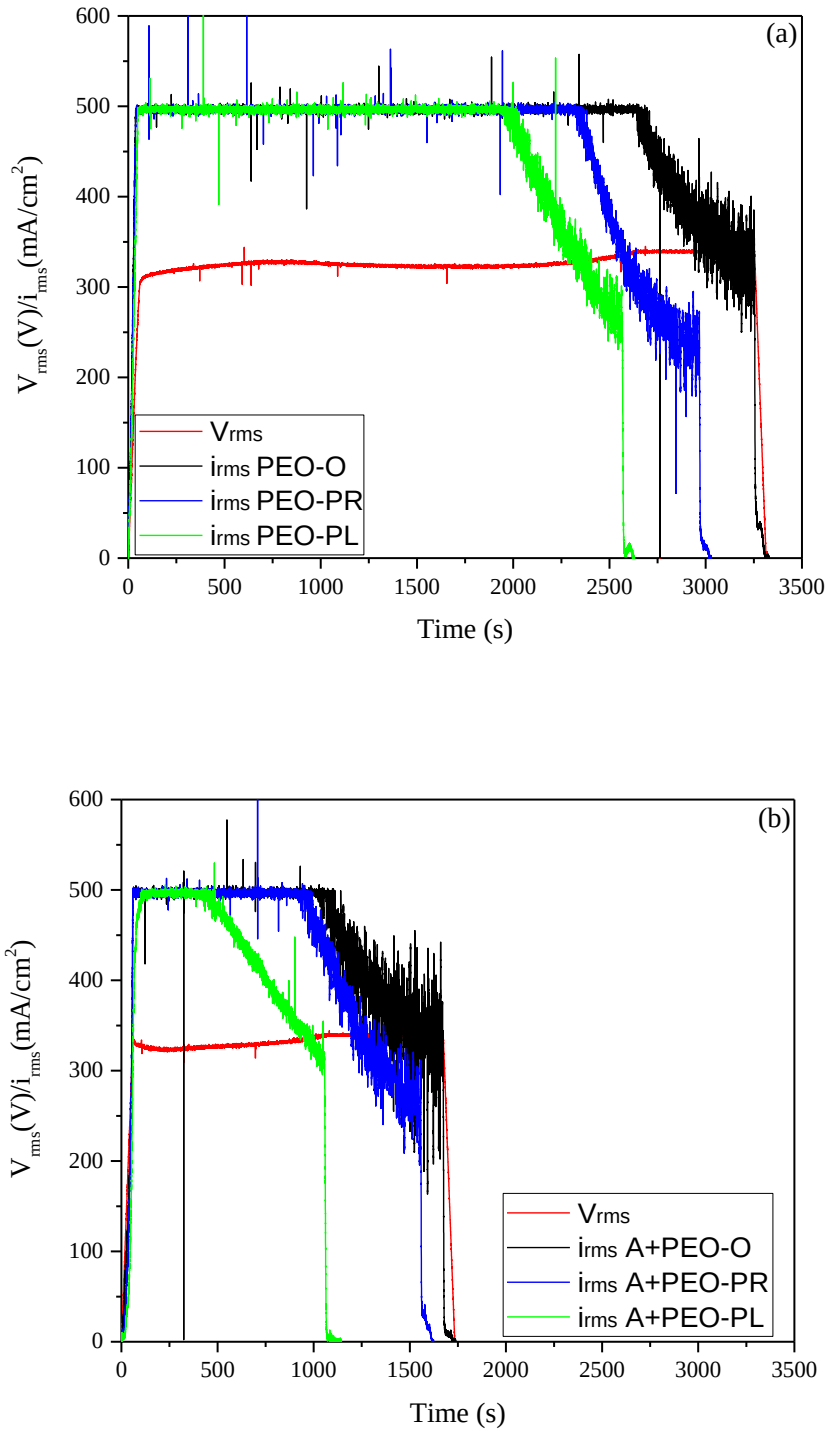


Figure 2. Rms current-time transients of PEO in different electrolytes for (a) direct PEO (b) PEO with precursor anodic film. Voltage values are also included for the electrolytes containing orthophosphate.

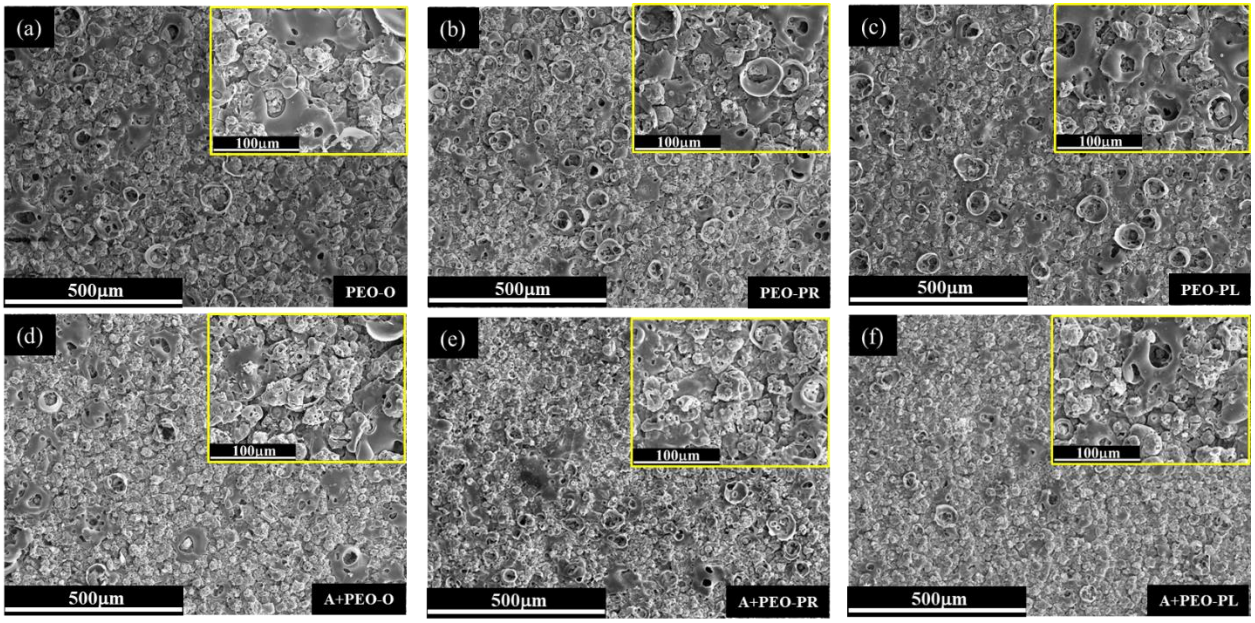


Figure 3. PEO coating surface view without precursor (a–c), and with precursors (d–f). Electrolytes: (a,d): ortophosphate (b,e): pyrophosphate (c,f): polyphosphate.

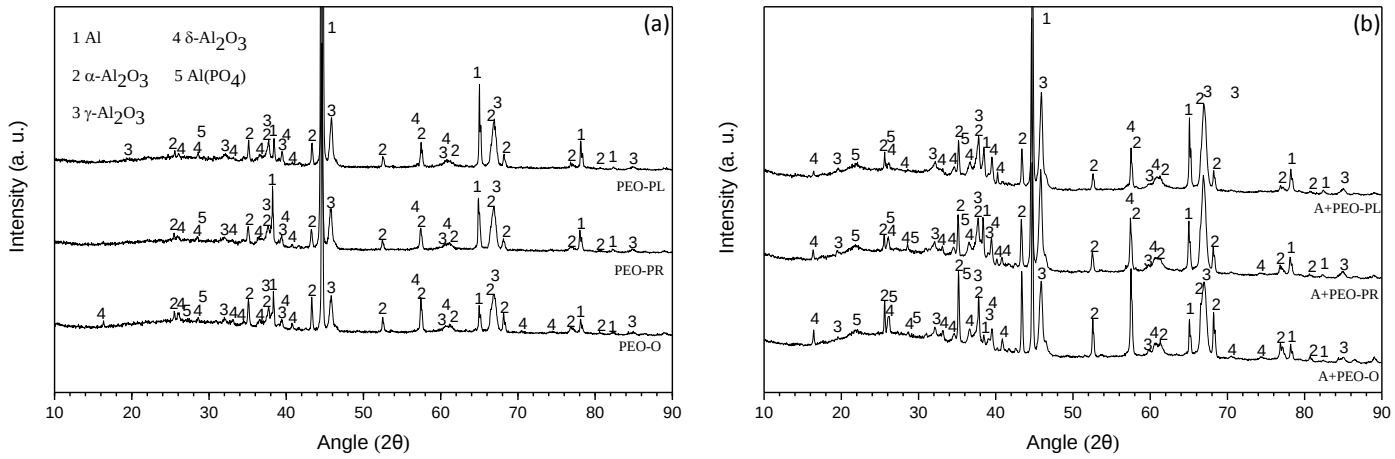


Figure 4. X-ray diffraction patterns of (a) PEO-O, PEO-PR and PEO-PL and (b) preanodized A+PEO-O, A+PEO-PR and A+PEO-PL coatings.

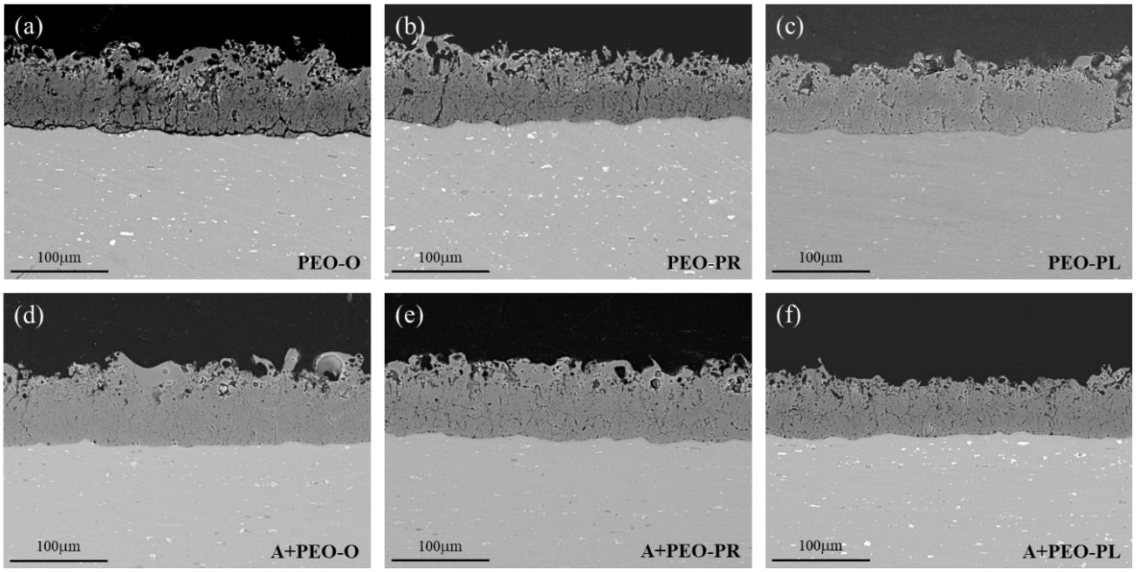


Figure 5. Backscattered electron images of the PEO coating cross-sections without precursor (a–c), and with precursors (d–f). Electrolytes: (a,d): silicate-ortophosphate (b,e): pyrophosphate (c,f): polyphosphate.

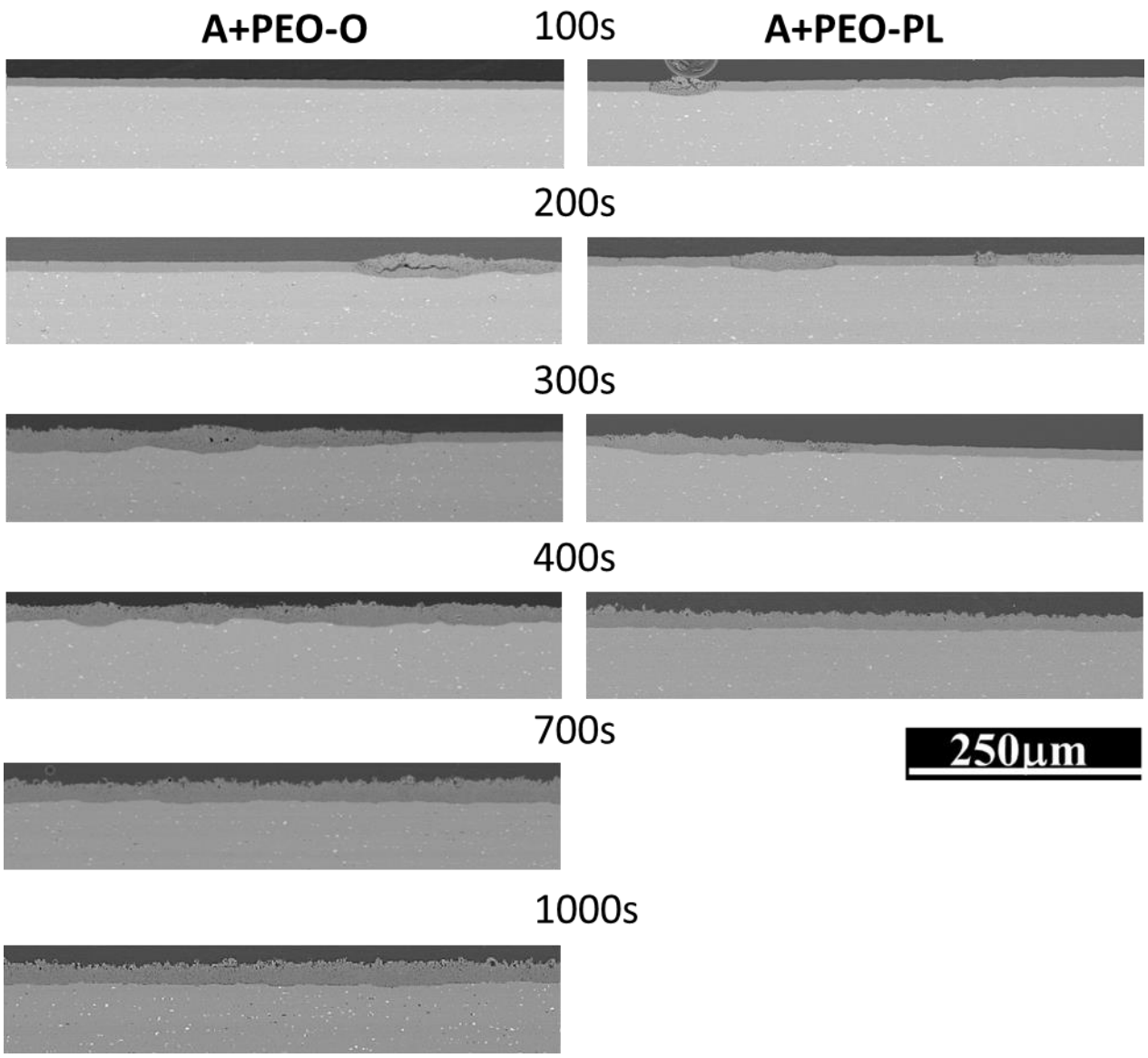


Figure 6. Partial transformation at different times of the preformed anodic film during PEO-O and PEO-PL process.

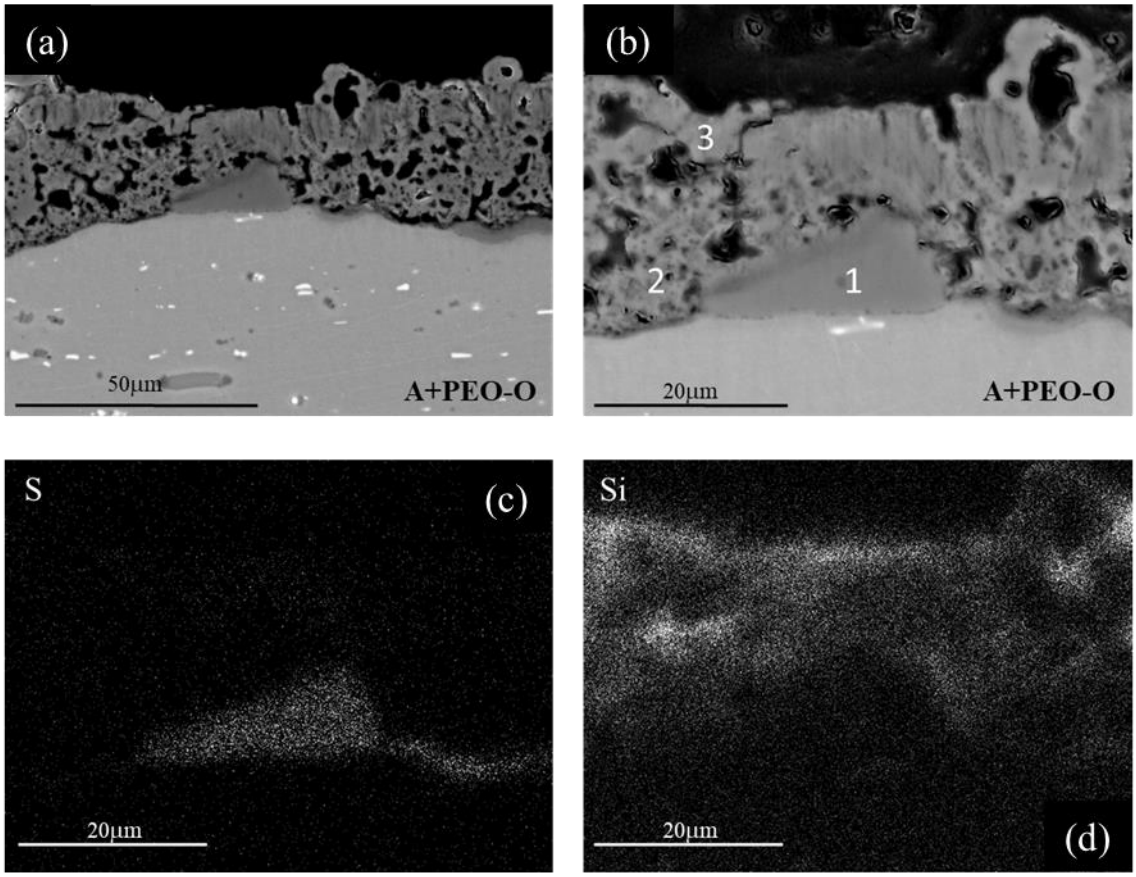


Figure 7. Backscattered electron micrographs of the PEO coating formed in silicate-orthophosphate electrolyte (400 s) with pre-anodized layer: (a) lower magnification, (b) higher magnification with its respective X-ray elemental maps of S and Si.

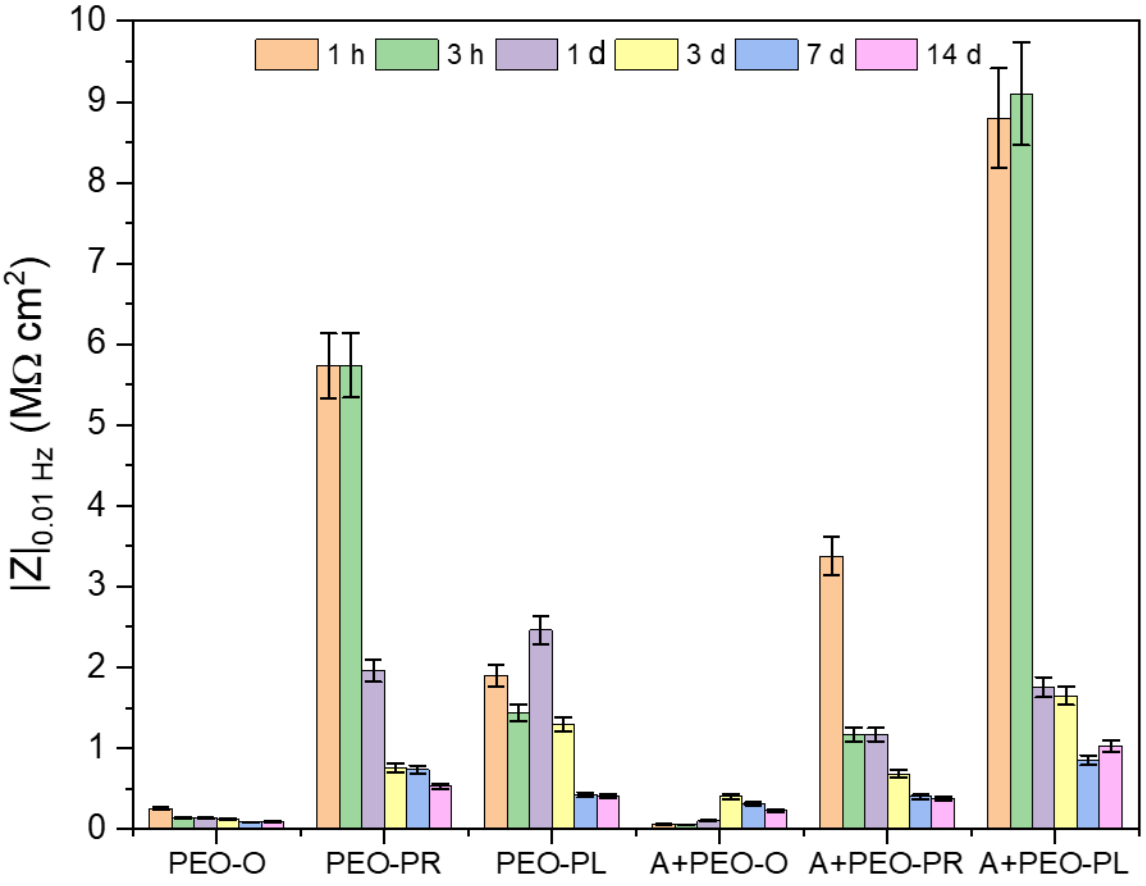


Figure 8. Total impedance at 0.01 Hz of the studied coatings as a function of the immersion time in naturally aerated NaCl 3.5 wt.% solution.

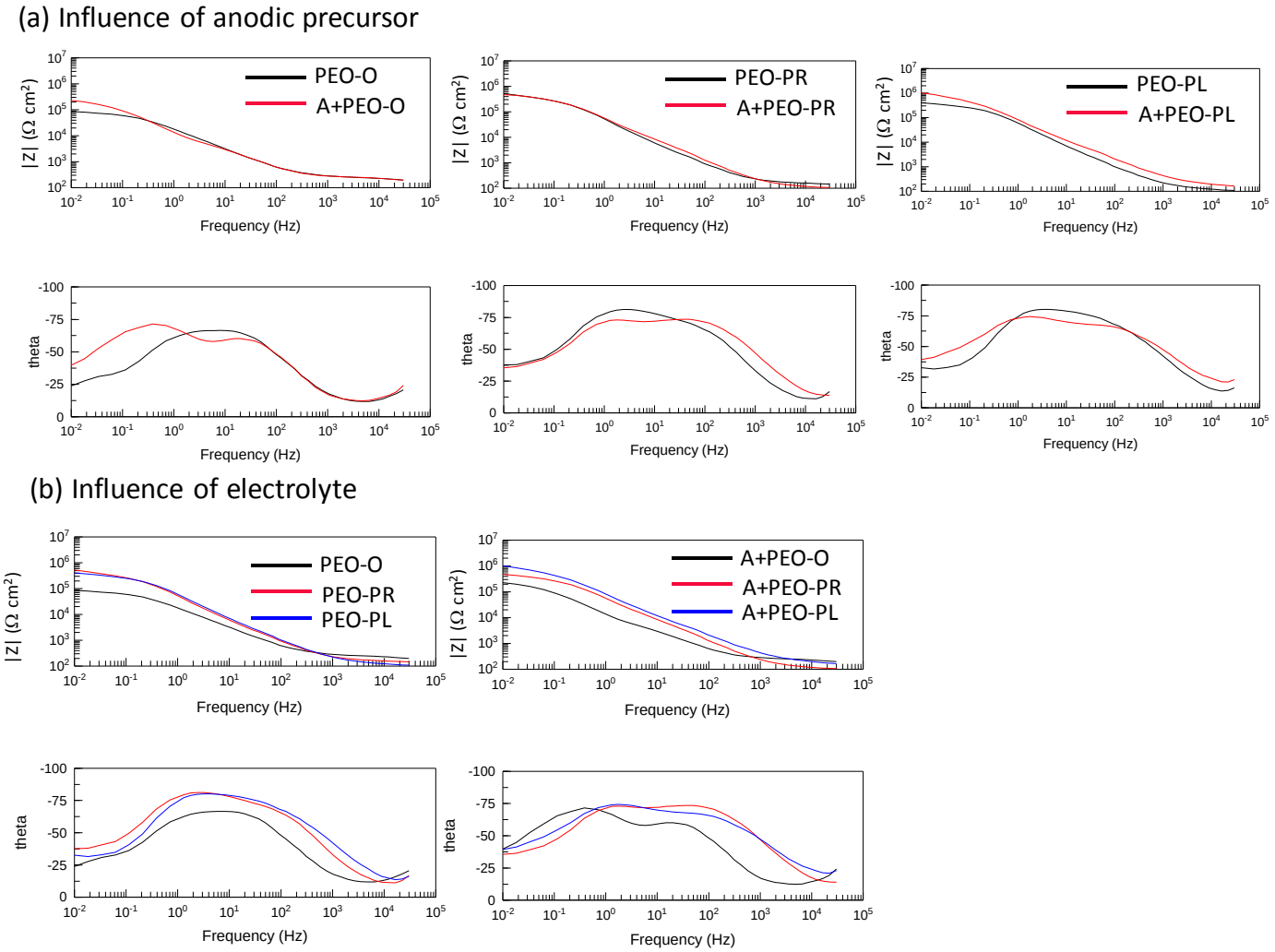


Figure 9. Bode plot of the studied coatings after 14 d of immersion in naturally aerated NaCl 3.5 wt. % solution as a function of (a) the anodic precursor and (b) electrolyte.

Graphical Abstract

**Influence of pre-anodizing**
Direct PEO vs. Pre-anodizing + PEO

**Influence PEO electrolyte**
Orthophosphate/Pyrophosphate/Polyphosphate

Best candidate: **Pre-anodizing + PEO-PL**

- Energy savings up to 60 %
- Good corrosion performance

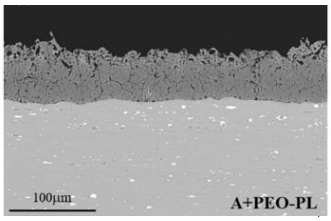


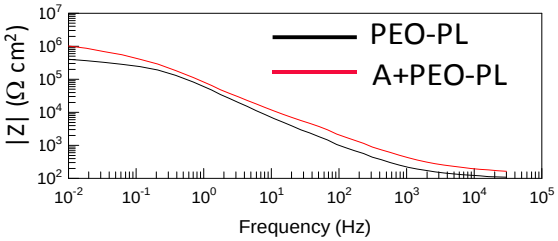


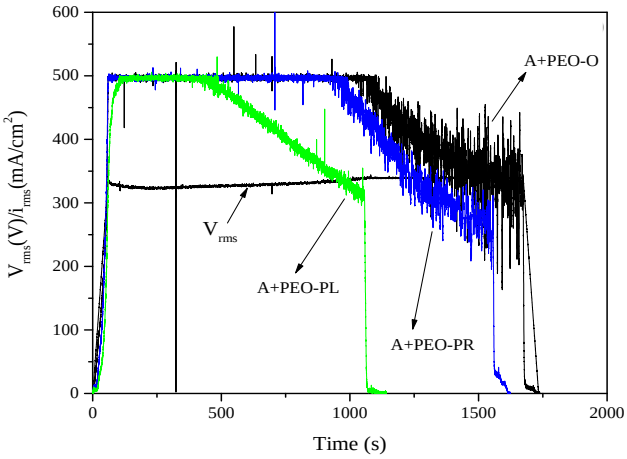

Author contributions:

Conceptualization: M. Mohedano, E. Matykina
Formal Analysis: M. Mohedano, E. Matykina, R. Arrabal
Methodology: M. Mohedano, B. Mingo, H. Mora-Sánchez
Resources: E. Matykina, R. Arrabal and M. Mohedano
Investigation: M. Mohedano, B. Mingo, H. Mora-Sánchez
Writing - Original Draft: M. Mohedano, B. Mingo
Writing - Review & Editing: E. Matykina, R. Arrabal, H. Mora-Sanchez
Funding acquisition: M. Mohedano, E. Matykina, R. Arrabal
Project Administration: M. Mohedano, R. Arrabal, E. Matykina

*Declaration of Interest Statement

**Declaration of interests**

☒ The authors declare that they have no known competing financial interests or personal relationships that could have appeared to influence the work reported in this paper.

☐The authors declare the following financial interests/personal relationships which may be considered as potential competing interests: